







# Energy Budget over Seasonal Snow Surface at an Open Site and Beneath Forest Canopy Openness during the Snowmelt Period in Western Tianshan Mountains, China

LU Heng<sup>1,2</sup>  <http://orcid.org/0000-0002-8289-6917>;  e-mail: luhengwzs@163.com

WEI Wen-shou<sup>3</sup>  <http://orcid.org/0000-0002-7195-7497>; e-mail: weiwsh@idm.cn

LIU Mingzhe<sup>4,4</sup>  <http://orcid.org/0000-0002-0291-2885>; e-mail: liumz@ms.xjb.ac.cn

HAN Xi<sup>3</sup>  <http://orcid.org/0000-0001-8139-5718>; e-mail: hanxi1105@163.com

HONG Wen<sup>1,2</sup>  <http://orcid.org/0000-0002-5997-6839>; e-mail: platypus11.11@163.com

<sup>1</sup> Xinjiang Institute of Ecology and Geography, Chinese Academy of Sciences, Urumqi 830011, China

<sup>2</sup> University of Chinese Academy of Sciences, Beijing 100049, China

<sup>3</sup> Institute of Desert Meteorology, China Meteorological Administration, Urumqi 830002, China

<sup>4</sup> Tianshan Station for Snow & Avalanche Research, Urumqi 830011, China

**Citation:** Lu H, Wei WS, Liu MZ, et al. (2015) Energy budget over seasonal snow surface at an open site and beneath forest canopy openness during the snowmelt period in western Tianshan Mountains, China. *Journal of Mountain Science* 12(2). DOI: 10.1007/s11629-014-3233-8

© Science Press and Institute of Mountain Hazards and Environment, CAS and Springer-Verlag Berlin Heidelberg 2015

**Abstract:** In this study, meteorological factors and snowmelt rate at an open site on sunny slope (OPS) and beneath forest canopy openness on shady slope (BFC) were measured using an automatic weather station and snow lysimeter during the snowmelt period in 2009, 2010 and 2013. The energy budget over snow surface was calculated according to these meteorological datasets. The analysis results indicated that the net shortwave radiation ( $K$ ) and sensible heat flux ( $H$ ) were energy sources, and the latent heat flux ( $L_vE$ ) was energy sinks of snow surfaces at all sites. The net longwave radiation ( $L$ ) was energy sink at OPS and 80% BFC, but energy source at 20% BFC. The gain of  $K$ ,  $H$ , and the loss of  $L_vE$  at BFC were obviously lower than those at OPS. The  $L$  was the maximum difference of energy budget between snow surface at BFC and OPS. In warm and wet years, the most important factor of the energy budget variation at OPS was air humidity and the second most

important factor was air temperature. However, the ground surface temperature on the sunny slope was the most important factor for  $L$  and energy budget at BFC. With the increases in forest canopy openness and the slope of adjacent terrains, the influences of ground surface temperature on the sunny slope on  $L$  and the energy budget over snow surface at BFC increased, especially when the snow cover on the sunny slope melts completely.

**Keywords:** Energy budget; Seasonal snow; Snowmelt period; Tianshan Mountains

## Introduction

Snow cover represents an important water resource for the Northern Hemisphere (Barnett et al. 2005; Viviroli et al. 2005). On the Tibetan Plateau and in the arid regions in Northwest China (Che et al.

**Received:** 30 July 2014  
**Accepted:** 18 December 2014

2005), snowmelt runoff is a vital resource and its allocation and management directly influences industrial and agricultural production and the ecological environment of the watershed (Bao et al. 2010). Site-level measurements of snow surface energy exchange and snowmelt are also critical for supporting basin snowmelt investigations and modeling (Cline 1997). Many people have reported the energy budget over the snow surface without forest canopy cover (De la Casiniere 1974; Moore et al. 1984; Calanca et al. 1990; Marks et al. 1992; McGregor et al. 1996; Aizen et al. 1997; Neale et al. 1997; Cline 1997; Sensoy et al. 2006). These results showed that the major energy budget difference among different regions lay in the percentages of components in total energy as well as the latent heat flux. Harding et al. (1996), Suzuki et al. (2003), Sicart et al. (2004), Boon (2009), Essery et al. (2008), and Burles et al. (2010) measured and analyzed the energy budget over the snow surface beneath the forest canopy. These measurement results showed that the  $H$  and  $L_vE$  over snow surface beneath the forest canopy decreased because canopies reduced wind speed. Moreover, canopies reduced the downward shortwave radiation and increased the longwave radiation. However, the increase in longwave radiation may be larger or smaller than the decrease in downward shortwave radiation. The above studies and analyses of the energy budget over snow surface were mainly conducted at open site or beneath forest canopy, where the characteristic of underlying surfaces was relatively uniform. However, the vegetation significantly varies with slopes in the study area, the sunny slope is mainly covered by subalpine meadow vegetation, the shady slope is mainly covered by *Picea Schrenkiana*, and the forest canopy openness on the shady slope is very small (Hu et al. 1997). Liu et al. (1989), Wei et al. (1996), Ma et al. (1991, 1993), and Liu et al. (1997) only investigated the energy budget over snow surface at the open site on sunny slopes. The energy budget over snow surface beneath forest canopy on shady slopes was not observed and analyzed.

Shi et al. (2002, 2003) demonstrated that the climate in northwest China since 1987 had changed from a warm-dry climate to a warm-wet climate. Unlike regions of the Tianshan Mountains outside of China, the Chinese range showed increased snowfall and snow cover days (Xu et al. 1996; Qin

et al. 2006; Annina et al. 2012). In the Chinese Tianshan Mountains, the increase in annual average air temperature was  $0.19^{\circ}\text{C}\sim 0.44^{\circ}\text{C}$   $10\text{a}^{-1}$  (Yuan et al. 2003, 2005; Yang et al. 2007; Wei et al. 2008). The increase in water vapor pressure from 1961 to 2009 was  $0.17$  hPa  $10\text{a}^{-1}$ . The water vapor pressure showed a consistent variation trend with average air temperature and precipitation (Yao et al. 2012). The variations of air temperature and humidity are different at open sites on the sunny slopes and beneath different forest canopy openness. The influences of climate change on the energy budget over snow surfaces and the snowmelt process may vary with environment. In the study, we observed and analyzed the energy budget over snow surfaces at an open site on a sunny slope and beneath different canopy openness on a shady slope in different years. The principal areas explored in this paper are: (1) the difference of energy budget over snow surfaces at the open site on a sunny slope and beneath forest canopy on a shady slope. (2) the influence of snow ablation on a sunny slope on the energy budget over snow surface beneath forest canopy on a shady slope. (3) the main influence factor of the energy budget over snow surface at an open site on a sunny slope and beneath different forest canopy openness.

## 1 Study Area and Methods

### 1.1 Study area

The study was conducted at Tianshan Station for Snow Cover and Avalanche Research, Chinese Academy of Sciences with the elevation of 1776 m above sea level ( $43^{\circ}16'\text{N}$ ,  $84^{\circ}24'\text{E}$ ). The station is located in the upstream branch of the Kunes River in the mid-mountain zone of the western Tianshan Mountains, China (Figure 1). Under the control of continental climate, the multi-year mean air temperature of the study area is  $1.3^{\circ}\text{C}$ , and the monthly average air temperature in January is  $-14.4^{\circ}\text{C}$ . Average annual precipitation is 867.3 mm, 30% of which is solid precipitation in the form of seasonal snowfall. The average annual maximum snow depth after 1976 was 78 cm, and the maximum value of 152 cm occurred during the winter from 2000 to 2001. Due to water erosion,

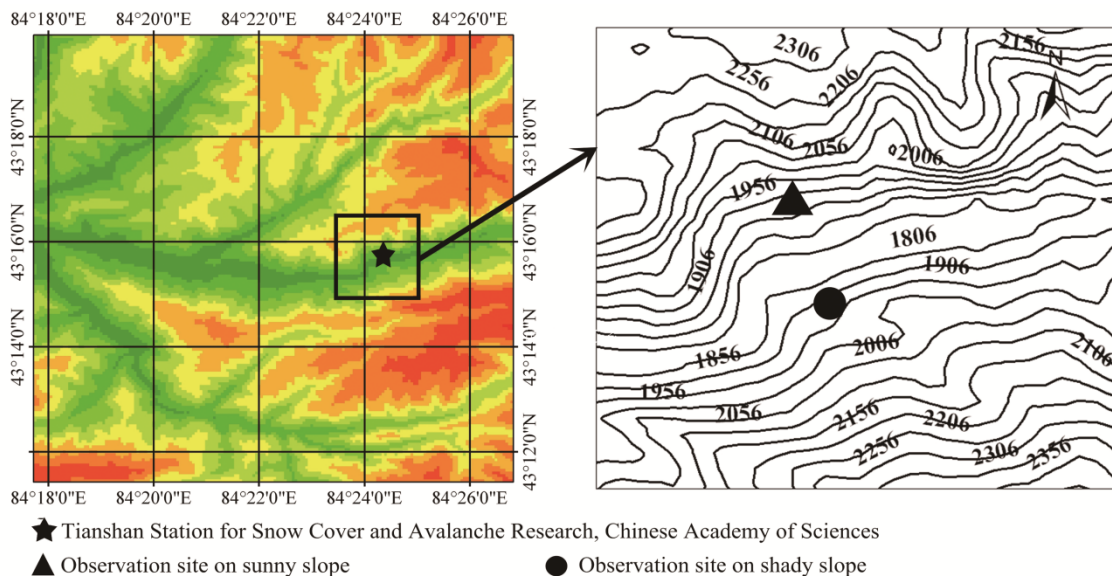


**Figure 1** Topography map depicting the study area and the observation site.

the main terrain form in the study area is the V-shaped valley. The valley floor is narrow and the incision depth ranges from 400 m to 600 m. The forest community structure is simple in the forest zone on the shady slope. The plant community has one dominant species, *Picea Schrenkiana*. The percentage (the ratio of the individual species to the total number of species) of *Picea Schrenkiana* is 89.38%; the percentage of *Sorbus tianschanica* is only 8.22%; that of other species is smaller than 1%. The canopy density is so high that the shrub layer is underdeveloped due to the light limitation and the representative species beneath forest canopy include *Aegopodium alpestre*, *Cicerbita azurea*, and *Dryopteris filix-mas* (Zhang et al. 2010). The study was conducted at an open site on a sunny slope (OPS) and beneath *Picea schrenkiana* forest canopy with 20% openness (20% BFC) and 80% openness (80% BFC) on a shady slope (Figure 1). The underlying surface at OPS is grassland without forest cover. The forest canopy openness was characterized with hemispherical photographs. The hemispherical photographs were analyzed by the Gap Light Analyzer (Version 2.0) software. The air temperature, humidity, wind speed, downward and upward shortwave radiation, and downward and upward longwave radiation were measured by automatic weather stations (Table 1). The snow water equivalent (SWE) was measured manually at OPS on the 5th, 10th, 15th, 20th, 25th, and the last day of every month from 1982 to 2013.

### 1.2 Surface energy balance

The snow surface energy balance equation is expressed as (Jin et al. 1999):

$$Q_m = K + L + H + L_v E + I_{prec} + G \quad (1)$$

where  $Q_m$  is the total energy ( $W\ m^{-2}$ );  $K$  is the net shortwave radiation ( $W\ m^{-2}$ );  $L$  is the net longwave radiation ( $W\ m^{-2}$ );  $H$  is the sensible heat flux ( $W\ m^{-2}$ );  $L_v E$  is the latent heat flux ( $W\ m^{-2}$ );  $I_{prec}$  is the energy supplied by precipitation (heat flux advected to the snowpack by rain or snow) ( $W\ m^{-2}$ );  $G$  is the ground heat flux ( $W\ m^{-2}$ ).  $I_{prec}$  and  $G$  were not considered in this study. In this paper, downward energy was positive and the energy was gained by the snowpack.

The sensible heat flux ( $H$ ) was calculated as a function of the temperature gradient above the snow surface (McKay and Thurtell 1978):

$$H = \rho_a C_{pa} K_* (T_a - T_{ss}) \quad (2)$$

where  $\rho_a$  is the density of air ( $kg\ m^{-3}$ );  $C_{pa}$  is the heat capacity of air ( $J\ kg^{-1}\ K^{-1}$ ); and  $K_*$  is the bulk transfer coefficient ( $m\ s^{-1}$ ). The snow surface temperature ( $T_{ss}$ ) was calculated according to the upward longwave radiation. When the calculated snow surface temperature ( $T_{ss}$ ) was higher than  $0^\circ C$ , the snow surface temperature was  $0^\circ C$ .

The latent heat flux ( $L_v E$ ) was calculated as a function of the vapor pressure gradient above the snow surface (McKay and Thurtell 1978):

**Table 1 Instruments used in this study and their nominal specifications**

Parameter	Symbol	Instrument	Range	Accuracy	Measurement heights (m)	Frequency (min)
Air temperature	$T_a$	Thermistor	-40~80 (°C)	±0.1 (°C)	1.5	30
Relative humidity	$RH$	Hygristor	0~100%	±2%	1.5	30
Wind speed	$u$	Propeller	0~50 (m s <sup>-1</sup> )	±0.2 (m s <sup>-1</sup> )	3	30
Atmosphere pressure	$P$	Capacitance	0~1200 (hPa)	±0.3 (hPa)	1.5	30
Longwave radiation	$L$	Pyrgeometer	3-50 (μm)	<3%	1.5	30
Shortwave radiation	$K$	Pyranometer	0.3-2.8 (μm)	<3%	1.5	30
Snowmelt rate(2009, 2010)	$r$	Electronic balance		1 (g)		
Snowmelt rate (2013)	$r$	Tipping bucket rain gauge		0.2 (mm)		

$$L_v E = \rho_a \lambda_v K_* \frac{0.622}{P} (e_a - e_{ss}) \quad (3)$$

where  $\lambda_v$  is the latent heat of vaporization ( $2.48 \times 10^6$  J kg<sup>-1</sup>);  $K_*$  is the bulk transfer coefficient ( $\text{m s}^{-1}$ );  $P$  is the atmospheric pressure (kPa); and  $e_a$  and  $e_{ss}$  are the atmospheric and snow surface vapor pressure (kPa), respectively. The atmosphere and snow surface vapor pressure were calculated with atmosphere and snow surface temperature according to the Magnus Formula. The range of  $z_0$  was from 2.5 mm to 10 mm during snowmelt period in many literatures (Sverdrup 1936; Grainger and Lister 1966; Moore and Owens 1984; Hay and Fitzharris 1987; Munro 1989; Hock and Holmgren 2005; Boon 2009). In this study, the  $z_0$  was equal to 6 mm according to Boon's study (2009). Thus, the errors of  $H$  and  $L_v E$  was caused by  $z_0$  was not bigger than 6%.

Under neutral atmospheric conditions (Anderson 1976; Male and Gray 1981):

$$K_N = \frac{k^2 u_a}{[\ln(\frac{z_a}{z_0})]^2} \quad (4)$$

where  $k$  is von Karman's constant (0.40);  $u_a$  is the wind speed ( $\text{m s}^{-1}$ );  $z_a$  is the wind height of the wind measurement (m);  $z_0$  is the roughness length of the snow surface (m).

Tarboton et al. (1995) used a correction for stable and unstable atmospheric stability following Price and Dunne (1976):

$$K_* = \begin{cases} K_N / (1 + 10 Ri), & Ri > 0 \\ K_N / (1 - 10 Ri) & Ri < 0 \end{cases} \quad (5)$$

where  $Ri$  is an estimate of the Richardson number,  $Ri > 0$  and  $Ri < 0$  is indicated stable and unstable atmospheric stability, respectively.

$$Ri = \frac{g(T_a - T_{ss})z_a}{u^2 [0.5(T_a + T_{ss}) + 273.15]} \quad (6)$$

where  $g$  is the acceleration due to gravity. However, due to the large temperature differences and low wind speeds results in unreasonable correction factors, according to results by Tarboton et al (1995), we have used neutral transfer coefficients in this study.

### 1.3 Snowmelt rate

The snowmelt rate was observed with lysimeter. A galvanized iron box (1 m × 1 m × 0.04 m) was placed at OPS, 80% BFC and 20% BFC before snowfall in winter. In 2009 and 2010, discharged water was collected in a plastic kettle and the discharged water was weighed every 2 h in the daytime and 1-3 times at night. The accuracy of the electronic balance was 0.001 kg. In 2013, the snowmelt rate was collected and measured using a tipping bucket rain gauge. The snowmelt period started on the day when discharged water was first observed through snow lysimeter (Table 2).

## 2 Results

### 2.1 Seasonal variation of snow water equivalent (SWE)

Figure 2a shows the variation of maximum SWE at the open site on the sunny slope from 1982 to 2013. The average maximum SWE was 178.4 mm with a standard deviation (SD) of 77.1 mm. The maximum SWE in 2009, 2010 and 2013 were 124 mm, 357 mm and 257 mm, respectively. Although the maximum SWE in 2009 was lower

**Table 2** The start and end time of snowmelt at the open site on the sunny slope and beneath different forest canopy openness on the shady slope

	At the open site			Forest canopy openness in 2013	
	In 2009	In 2010	In 2013	Beneath 80%	Beneath 20%
The start time	Mar 11	Mar 9	Feb 23	Mar 20	Mar 13
The end time	Mar 30	Apr 26	Mar 28	Apr 26	Apr 16

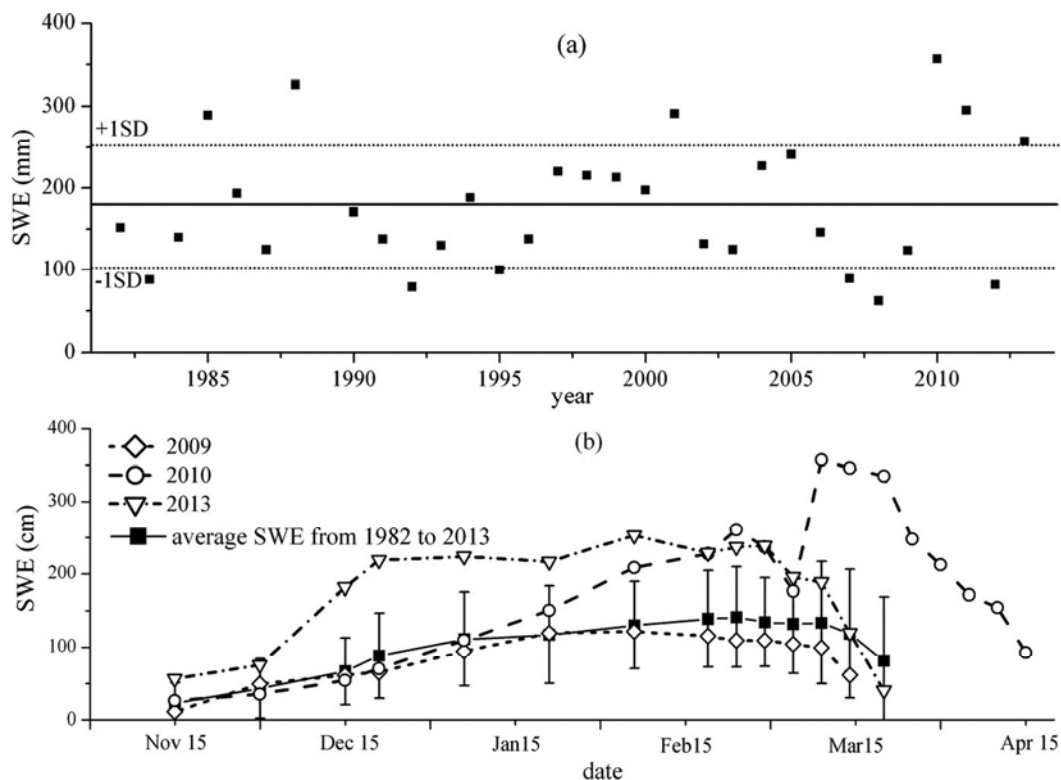


**Figure 2** The variation of snow water equivalent (SWE) at open site during 1982~2013, (a) the maximum SWE, (b) the SWE in 2009, 2010, 2013 and average SWE from 1982 to 2013, the error bar shows the standard deviation of SWE from 1982 to 2013.

than annual average SWE, it was within one SD. The maximum SWE in 2010 and 2013 were higher than the average SWE and above one SD. Especially, the maximum SWE in 2010 was the highest from 1982 to 2013. The variation of SWE in 2009 was similar to that of the annual average SWE and the SWE in 2009 was always within one SD. In 2010, the variation of SWE was similar to that of the annual average SWE in the early period. However, after Jan 31, 2010, the SWE was larger than the annual average SWE and above one SD. In 2013, the SWE was larger than the annual average SWE and above one SD in the early period, but within one SD in the later period. The SWE during snowmelt period in 2013 decreased more drastically than the average SWE (Figure 2b). Thus, the snow accumulation and ablation process were normal in 2009. The snowfall was abnormally high

in 2010 and 2013, but the abnormal snowfall in 2010 and 2013 mainly occurred during the snowmelt period and the accumulation period, respectively.

### 2.2 Variations of meteorological factors

The average air temperatures and specific humidity at OPS during the snowmelt period in 2010 and 2013 was higher than those in 2009. Thus, the climate during the snowmelt period in 2010 and 2013 was warmer and wetter than that in 2009 (Figure 3a~3c). The differences of wind speed at OPS among different years were not marked. The maximum wind speed was lower than 5 m s<sup>-1</sup> and the average wind speeds in 2009, 2010 and 2013 were 1.10 m s<sup>-1</sup>, 1.16 m s<sup>-1</sup>, and 0.89 m s<sup>-1</sup>, respectively.

Due to the influences of terrain and vegetation, the air temperature beneath forest canopy on the shady slope was lower than that at OPS in the same period. However, the start time and the end time of the snowmelt period at BFC was about 20~30 days later than that at OPS (Table 1), the average air temperatures during snowmelt period at 80% BFC and 20% BFC in 2013 were respectively 4.25°C and 2.11°C, which were clearly higher than that at OPS (Figure 3c~3e). Generally, the nighttime average air temperature at OPS was lower than 0°C, but the nighttime average air temperatures at 80% BFC and 20% BFC were respectively 1.31°C and 0.17°C. In 2013, the average specific humidity at 80% BFC and 20% BFC were respectively 5.03 g kg<sup>-1</sup> and 4.74 g kg<sup>-1</sup>, which were higher than that at OPS, 3.62 g kg<sup>-1</sup>. Thus, the climate during the snowmelt period beneath forest canopies during snowmelt period was warmer and wetter than that at the open site on the sunny slope. The average wind speed at 80% BFC and 20% BFC were clearly lower

than that at OPS.

### 2.3 The characteristic of the energy budget

#### 2.3.1 Variations of *K*, *L*, *H*, and *L<sub>v</sub>E*

Figure 4 shows the radiation over snow surface during the snowmelt period. The *K* gradually increased during the snowmelt period and decreased in the short term after snowfall. The *L* was generally negative for the emissivity of snow was larger than that of air. The *L* was close to 0 W m<sup>-2</sup> on cloudy or precipitation days. The average *K* and *L* at OPS in 2010 were lower than that in 2009. But the average net radiation (*K*+*L*) in 2010 was 1 W m<sup>-2</sup> higher than in 2009. The starting time of snowmelt at OPS in 2013 was earlier than that in 2009 (Table 2). Therefore, the average *K* in 2013 was lower than that in 2009. Furthermore, the dominant weather condition during the snowmelt period in 2013 was clear and the loss of *L* in 2013 was 3 W m<sup>-2</sup> less than that in 2009. The average

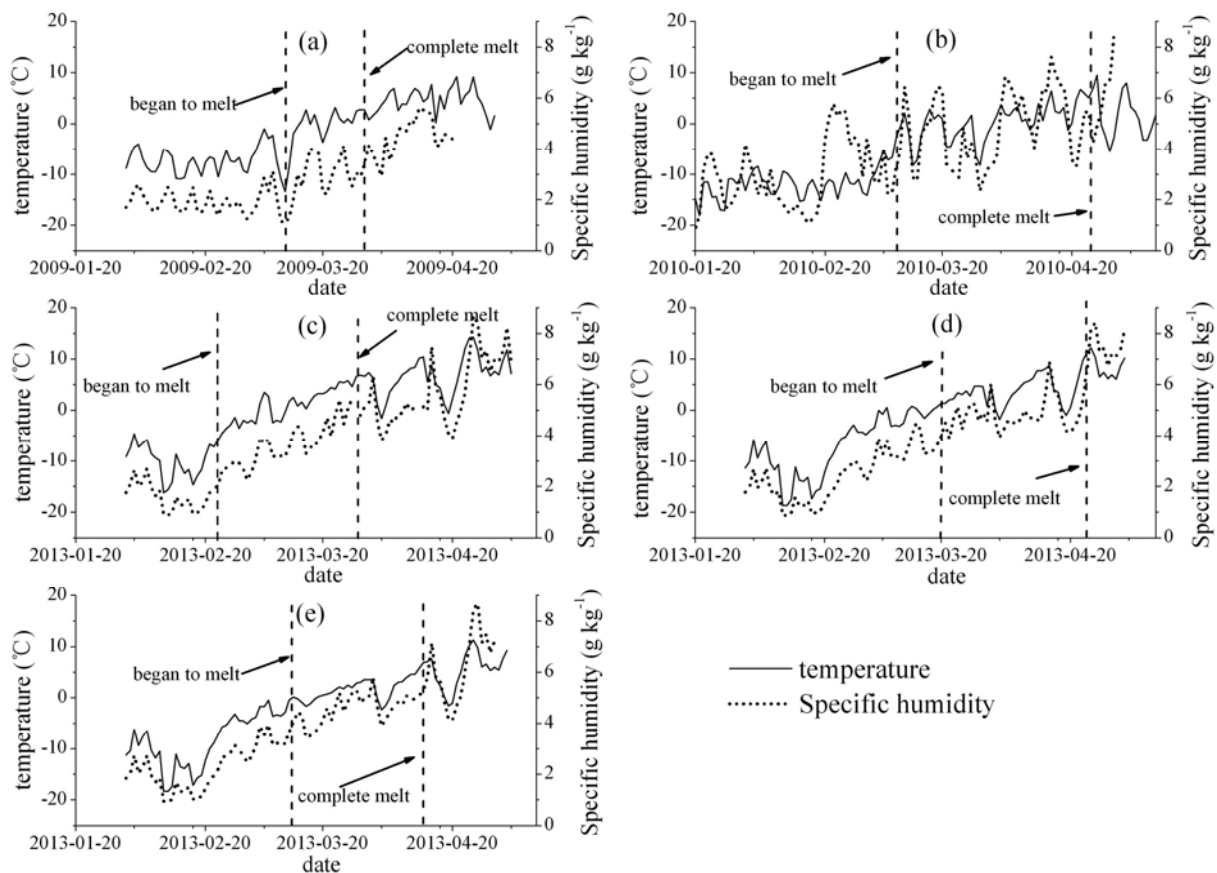


**Figure 3** Daily average air temperature and specific humidity patterns observed during the different snowmelt periods, (a) at open site on the sunny slope in 2009, (b) at open site on the sunny slope in 2010, (c) at open site on the sunny slope in 2013, (d) beneath 80% forest canopies on the shady slope in 2013, (e) beneath 20% forest canopies on the shady slope in 2013.

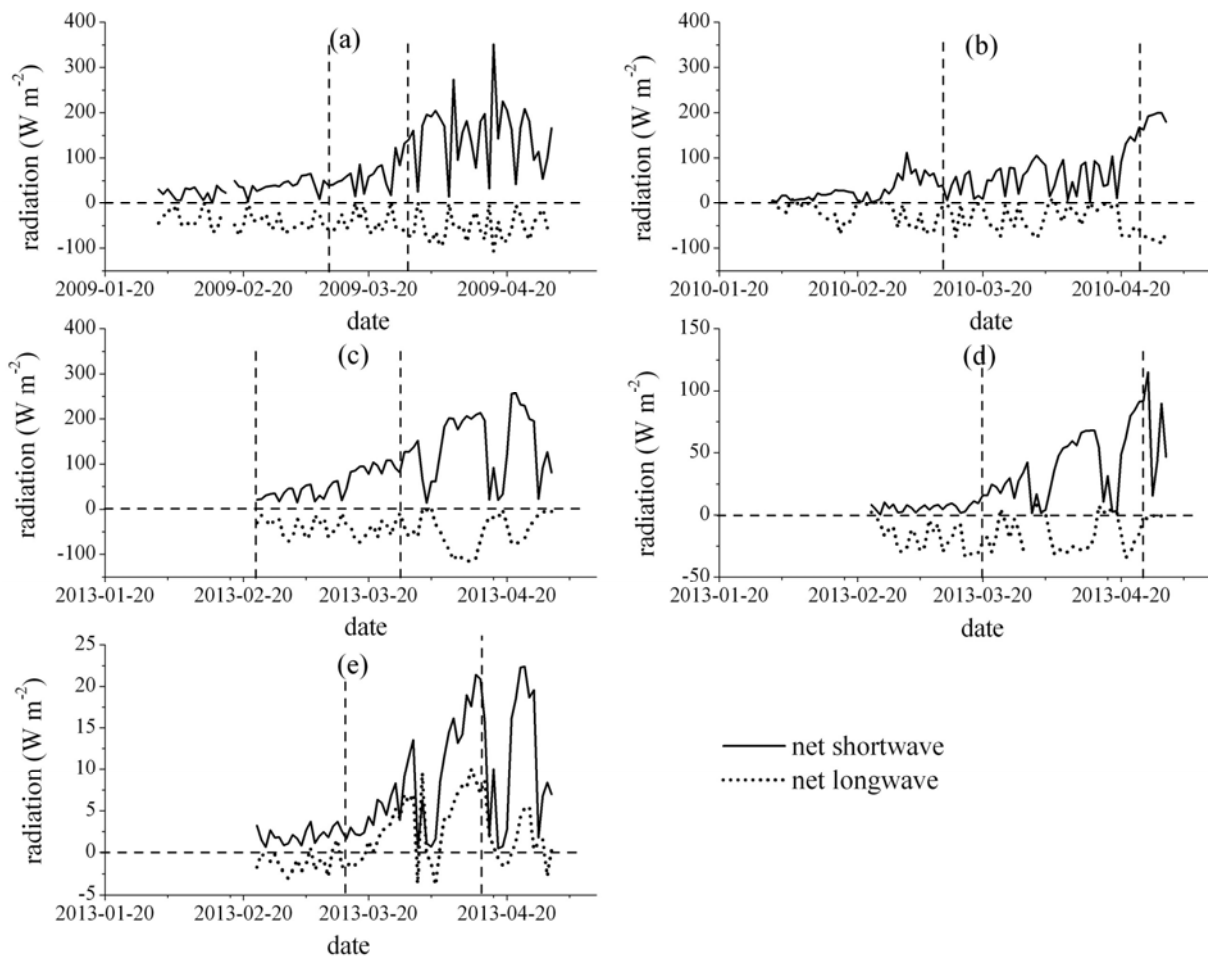


**Figure 4** Daily average net shortwave and longwave radiation patterns observed during the different snowmelt periods, (a) at open site on the sunny slope in 2009, (b) at open site on the sunny slope in 2010, (c) at open site on the sunny slope in 2013, (d) beneath 80% forest canopies on the shady slope in 2013, (e) beneath 20% forest canopies on the shady slope in 2013.

net radiation at the open site on the sunny slope in 2013 was  $13 \text{ W m}^{-2}$  lower than in 2009. Although the average snow surface albedo (calculated according to the measured downward and upward shortwave radiation) at 80% BFC and 20% BFC in 2013 were respectively 0.48 and 0.43, which were clearly lower than that at OPS, 0.63. The average  $K$  at 80% BFC and 20% BFC in 2013 were  $41 \text{ W m}^{-2}$  and  $8 \text{ W m}^{-2}$ , which were lower than that at OPS,  $58 \text{ W m}^{-2}$ , due to the influence of vegetation and terrain. The average  $L$  at 80% BFC was only  $-15 \text{ W m}^{-2}$ , which was significantly less than that at OPS. The average  $L$  at 20% BFC even reached  $3 \text{ W m}^{-2}$  (Figure 4d~4e).

Because the air temperature was generally higher than snow surface temperature, the  $H$  was positive. The sublimation process was the dominant process in snowmelt period, the  $L_vE$  was

negative and drastically increased in the later snowmelt period (Figure 5). The average  $H$  over the snow surface at OPS in 2009, 2010, and 2013 were respectively  $12 \text{ W m}^{-2}$ ,  $14 \text{ W m}^{-2}$ , and  $20 \text{ W m}^{-2}$ . The  $H$  in 2013 was significantly higher than that in other years. The differences in the temperature gradient (between air and snow surface) and wind speed between 2009 and 2010 were relatively small, resulting in the relatively small difference of  $H$ . For the climate at OPS in 2010 and 2013 was wetter than that in 2009, snow sublimation was impeded. The average  $L_vE$  at OPS in 2010 and 2013 were respectively  $-13 \text{ W m}^{-2}$  and  $-8 \text{ W m}^{-2}$ , which were significantly lower than that in 2009,  $-29 \text{ W m}^{-2}$  (Figure 5a~5c). Although the average air temperature at BFC during the snowmelt period in 2013 was higher than that at OPS, the average  $H$  over snow surfaces at 80% BFC and 20% BFC were

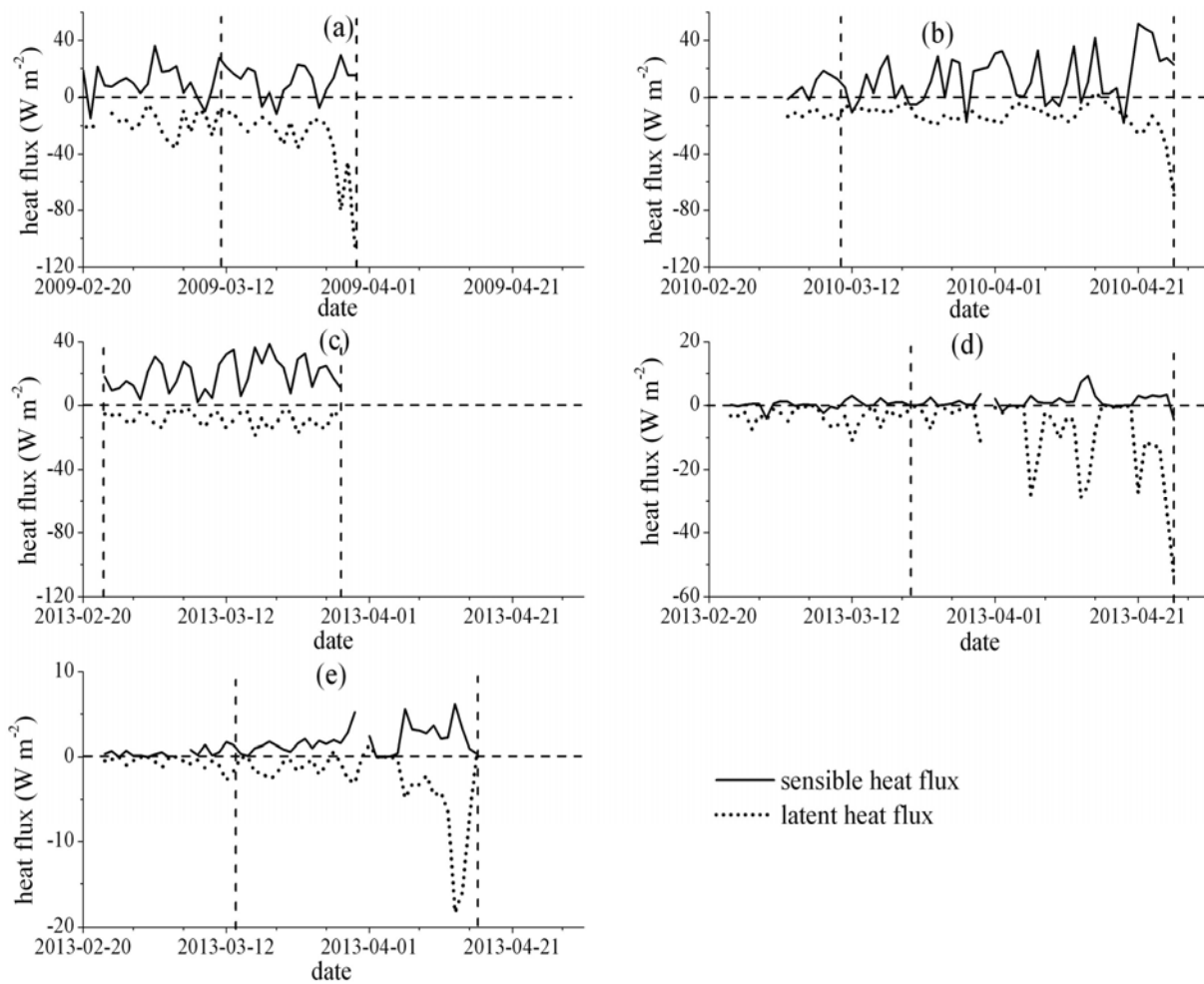


**Figure 5** Daily average sensible and latent heat fluxes patterns observed during the different snowmelt periods, (a) at open site on the sunny slope in 2009, (b) at open site on the sunny slope in 2010, (c) at open site on the sunny slope in 2013, (d) beneath 80% forest canopies on the shady slope in 2013, (e) beneath 20% forest canopies on the shady slope in 2013.

respectively  $1 \text{ W m}^{-2}$  and  $2 \text{ W m}^{-2}$ , which were clearly less than that at OPS,  $20 \text{ W m}^{-2}$ , because the wind speed beneath forest was lower than that at OPS. The average  $L_vE$  at 80% BFC and 20% BFC were  $-7 \text{ W m}^{-2}$  and  $-3 \text{ W m}^{-2}$ , which were less than that at OPS (Figure 5c~5e). The net turbulence over the snow surface at BFC was negative.

**2.3.2 Variation of cumulative energy by K, L, H, and LVE**

The fluxes of  $K$ ,  $L$ ,  $H$ , and  $L_vE$  in different years were integrated to determine the total energy contribution of each component in the snowmelt period. Over the snow surface at OPS and at 80% BFC,  $K$  and  $H$  were energy sources,  $L$  and  $L_vE$  were energy sinks (Table 3). The percentage of  $H$  vis-à-vis energy gain ( $K+H$ ) at OPS in 2013 was larger

than those in 2009 and 2010 (Table 3). The  $K$  was the most important source for the gain energy At 80% BFC and the percentages of the  $K$  and  $H$  vis-à-vis energy gain were respectively 96.8% and 3.2%.

**Table 3** The cumulative net shortwave radiation ( $K$ ), net longwave radiation ( $L$ ), sensible heat flux ( $H$ ) and latent heat flux ( $L_vE$ ) during snowmelt period ( $\text{MJ m}^{-2}$ )

Year	$K$	$L$	$H$	$L_vE$
2009, open site	115.41	-69.95	21.17	-49.76
2010, open site	315.50	-156.79	58.69	-55.24
2013, open site	160.33	-113.32	56.37	-23.53
2013, 80% canopy	127.68	-47.10	4.20	4.20
2013, 20% canopy	23.11	23.11	23.11	23.11

**Note:** 20% and 80% canopy refers to that the measurement was conducted at the site beneath 20% and 80% forest canopy openness.



At 20% BFC, the percentages of  $K$ ,  $L$  and  $H$  vis-à-vis energy gain ( $K+L+H$ ) were 60.0%, 25.5%, and 15.0%. The loss of  $L$  was higher than the loss of  $L_vE$  at OPS and 80% BFC. The percentage of  $L_vE$  vis-à-vis energy loss ( $L+L_vE$ ) at OPS in 2010 and 2013 were respectively 26.05% and 16.1%, which were markedly smaller than that in 2009(41.6%). However, the percentage of  $L_vE$  vis-à-vis energy loss at 80% BFC was 36.6%, which was markedly higher than at OPS in 2013, 16.1%.

### 3 Discussion

#### 3.1 The energy budget at OPS

The snowmelt period in the abnormally high snowfall years (2010 and 2013) at OPS was warmer and wetter than that in the normal snowfall year (2009), thus changing  $H$  and  $L_vE$  over the snow surface. The  $H$  at OPS in 2010 and 2013 was higher than that in 2009, but the losses of  $L_vE$  in 2010 and 2013 were lower than that in 2009. Therefore, the total energy over the snow surface and snowmelt rate in 2010 and 2013 increased. For example, the average snowmelt rates at OPS in the whole snowmelt period in 2010 and 2013 were respectively 10.46 mm d<sup>-1</sup> and 11.00 mm d<sup>-1</sup>, higher than in 2009, 7.82 mm d<sup>-1</sup>. Especially, the snowmelt rates during the later snowmelt period in 2010 and 2013 were significantly higher than that in 2009. For example, in the last 15 days of the snowmelt period, the average snowmelt rates in 2010 and 2013 were 24.04 mm d<sup>-1</sup> and 24.82 mm d<sup>-1</sup>, which were clearly higher than that in 2009, 10.36 mm d<sup>-1</sup> (Figure 6).

In the warmer and wetter years (2010 and 2013) and the normal year (2009), the difference of  $L_vE$  at OPS was larger than the difference of  $H$ . For example, in 2010, the losses of  $L_vE$  in the whole day and daytime were respectively 15 W m<sup>-2</sup> and 30 W m<sup>-2</sup> lower than those in 2009 (Figure 7b). In 2013, the losses of  $L_vE$  in the whole day and daytime were 20 W m<sup>-2</sup> and 32 W m<sup>-2</sup> lower than those in 2009 (Figure 7c). However, the  $H$  in 2010 and 2013 were only 2 W m<sup>-2</sup> and

8 W m<sup>-2</sup> higher than that in 2009. Thus, the difference between the energy budget over snow surface at OPS in the warmer and wetter years and the energy budget in normal years was mainly caused by air humidity.

The average  $H$  over snow surface in 2013 and 2010 were 8 W m<sup>-2</sup> and 2 W m<sup>-2</sup> higher than in 2009. The difference in  $H$  between 2010 and 2013 was mainly caused by two factors: the asymmetric temperature rise between daytime and nighttime and the characteristic of snow surface temperature. When the air temperature was not higher than 0°C, snow surface temperature showed a good linear relationship with air temperature. However, the snow surface temperature could not increase with air temperature when air temperature was higher than 0°C. The  $H$  significantly increased with air temperature rise when air temperature higher than 0°C. The average daytime and nighttime temperatures in 2010 were respectively 0.04°C and 0.77°C higher than those in 2009. The average daytime and nighttime temperatures in 2013 were respectively 0.25°C and 0.31°C higher than those in 2009. In general, the average nighttime air temperature in all the observation years was lower than 0°C. Although the nighttime air temperature rise was marked in 2010, the influence of air temperature rise on  $H$  was not significant. For the daytime air temperature during snowmelt was generally higher than 0°C, the average  $H$  over snow surface in the daytime in 2013 was 11 W m<sup>-2</sup> higher than that in 2009 and the average  $H$  over snow surface in the daytime in 2010 was only 1 W m<sup>-2</sup>

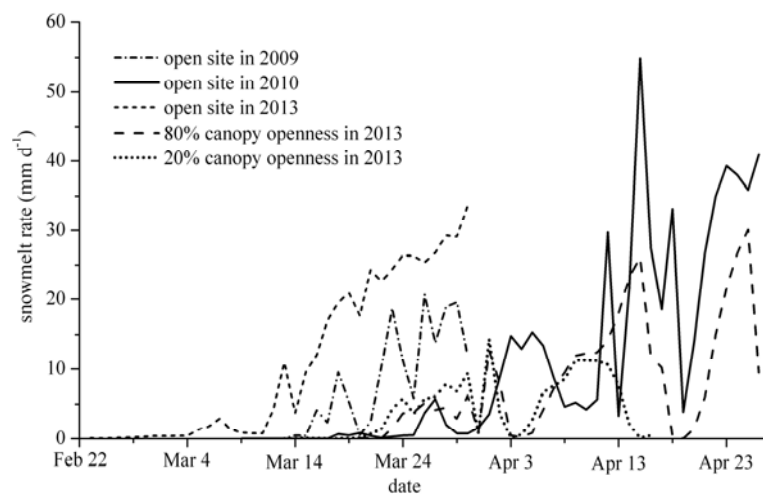


**Figure 6** The snowmelt rate for different underlying surface in different years.

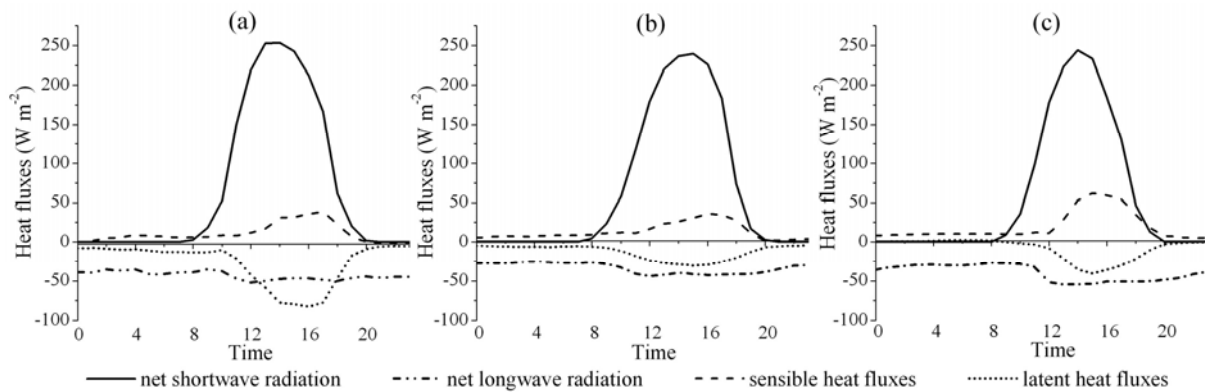


**Figure 7** The daily variation of  $K$ ,  $L$ ,  $H$  and  $L_vE$  at open site on the sunny slope in different years, (a) 2009, (b) 2010, (c) 2012.

higher than that in 2009 (Figure 7).

### 3.2 The energy budget at BFC

Radiation was the most important energy source over snow surface beneath forest canopy on the shady slope (Table 2). In 2013, the percentages of radiation *vis-à-vis* energy gain over snow surface at 80% BFC and 20% BFC were respectively 96.8% and 85.5%, which were clearly greater than that at OPS, 74.0%. Although the  $K$  at BFC was clearly lower than that at OPS due to the influence of vegetation and terrain, the loss of  $L$  at 80% BFC was 25  $W\ m^{-2}$  lower than at OPS. The  $L$  at 20% BFC was even positive and the difference between  $L$  at 20% BFC and  $L$  at OPS was 43  $W\ m^{-2}$ . The difference of  $L$  was mainly caused by the downward longwave radiation ( $L_{\downarrow}$ ). Generally, the canopies warmed by shortwave radiation and then enhanced the  $L_{\downarrow}$  (Rowlands et al. 2002). Furthermore, the  $L_{\downarrow}$  was also enhanced by adjacent terrain (Sicart et al. 2006) due to the dimensionless effective emissivity for adjacent terrain ( $\sim 0.98$  or  $0.94$ ) higher than the dimensionless effective emissivity for air ( $\sim 0.7$ ). Thus, the  $L_{\downarrow}$  beneath forest canopy on the shady slope could be divided into four components: the component passing through the canopy gap from the sky, the component emitted by the canopies, longwave radiation beneath forest canopy from the canopies which absorbed shortwave radiation and was above the air temperature, and the component enhanced by adjacent terrain (Figure 8). The  $L_{\downarrow}$  beneath forest canopy on the shady slope is given as (Lu et al. 2014):

$$L_{\downarrow} = v(\sigma_a \delta T_a^4) + (1-v)(\sigma_c \delta T_a^4) + \tau_s S_0 + \tau_l L_t + \zeta \quad (7)$$

where  $v\sigma_a \delta T_a^4$  indicates the longwave radiation passing through the canopies from the sky;  $(1-v)(\sigma_c \delta T_a^4)$  indicates the longwave radiation beneath forest canopy from the canopies at air temperature;  $\tau_s S_0$  indicates the longwave radiation beneath forest canopy from the canopies which absorbed shortwave radiation and was above the air temperature;  $\tau_l L_t$  indicates the longwave radiation beneath forest canopy enhanced by adjacent terrains;  $\delta$  is the Stefan-Boltzmann constant ( $5.670303 \times 10^{-8}\ W\ m^{-2}\ K^{-4}$ );  $\sigma_a$  and  $\sigma_c$  are dimensionless effective emissivity for sky and canopies ( $0.98$ );  $\sigma_a$  was calculated according to cloud cover (Iziomon et al. 2003),  $v$  is the forest

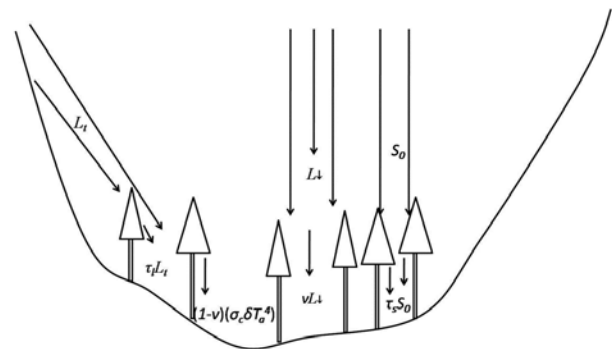


**Figure 8** The schematic to show downward longwave radiation over snow surface beneath forest canopy. (Notes:  $L_t$  is the longwave radiation enhanced by adjacent terrain above forest canopy,  $vL_{\downarrow}$  is the longwave radiation passing through the canopies from the sky,  $L_{\downarrow}$  is the longwave radiation from sky,  $\tau_l L_t$  is the longwave radiation beneath forest canopy enhanced by adjacent terrains,  $(1-v)(\sigma_c \delta T_a^4)$  is the longwave radiation beneath forest canopy from the canopies at air temperature,  $\tau_s S_0$  is the longwave radiation beneath forest canopy from the canopies which absorbed shortwave radiation and was above the air temperature,  $S_0$  is the downward shortwave radiation above forest canopies).

canopy openness;  $T_a$  is air temperature;  $S_o$  is the downward shortwave radiation above forest canopies;  $\tau_s$  is a dimensionless parameter for the conversion from shortwave radiation absorbed by canopy to downward longwave radiation;  $\tau_l$  is a dimensionless parameter indicating the influences of the longwave radiation enhanced by adjacent terrain on downward longwave radiation beneath forest canopies;  $L_t$  is the longwave radiation enhanced by adjacent terrain;  $\xi$  is the error.

The longwave radiation enhanced by adjacent terrain above forest canopy ( $L_t$ ) is given by

$$L_t = L_{\downarrow} - \sigma_a \delta T_a^4 \tag{8}$$

where  $L_{\downarrow}$  is the measured downward longwave radiation at the open site on the sunny slope.

The values of  $\tau_s$  and  $\tau_l$  were fitted according to the Eq.(7) using the observed hourly downward longwave radiation beneath forest canopy. According to the simulation results of Eq.(7), at 80% BFC and 20% BFC,  $\tau_s$  values were 0.006 and 0.017 and  $\tau_l$  values were 0.485 and 0.130, respectively. The RMSE of simulated  $L_{\downarrow}$  at 80% BFC and 20% BFC were 11.70 W m<sup>-2</sup> and 6.67 W m<sup>-2</sup>, respectively. The error of simulated  $L_{\downarrow}$  at 80% BFC and 20% BFC were respectively 13.08 W m<sup>-2</sup> and 5.30 W m<sup>-2</sup>. Thus, the  $L_{\downarrow}$  over snow surface beneath forest canopy can be better simulated with Eq. (7) (Lu et al. 2014). According to Eq. (7), the  $L_{\downarrow}$  over snow surface beneath forest canopy was mainly influenced by air temperature,  $S_o$ , and  $L_t$ . During the snowmelt period, the  $\tau_l L_t$  at 80% BFC and 20% BFC were respectively 21 W m<sup>-2</sup> and 5 W m<sup>-2</sup>, which were higher than  $H$ ,  $L_v E$ , and  $\tau_s S_o$ , especially at 80%

BFC. During the earlier snowmelt period or precipitation days,  $\tau_l L_t$  was even higher than  $K$  at BFC (Figure 9). Thus, the  $L_t$  is very important for the energy budget over snow surface at BFC.

The downward longwave radiation enhanced by adjacent terrain above forest canopy is calculated as (Sicart et al. 2006):

$$L_t = (1 - V_f) \sigma_s \delta T_s^4 \tag{9}$$

where  $V_f$  is the sky view factor (the larger slope in adjacent terrain and the steeper adjacent terrain means the smaller  $V_f$ );  $\sigma_s$  is the dimensionless effective emissivity for ground surface;  $T_s$  is the ground surface temperature. In the study area, the terrain was mainly V-shaped valley due to water erosion. Thus,  $L_t$  is given as:

$$L_t = 0.5(1 - V_f) \sigma_s \delta T_s^4 + 0.5(1 - V_f) \sigma_c \delta T_c^4 \tag{10}$$

Snow surface and ground surface without snow cover are different in the temperature and the dimensionless effective emissivity. The percentage of snow cover area on the sunny slope ( $F$ ) was decreased with snow depletion. Therefore, the enhanced longwave radiation by sunny slope can be divided into two parts: snow cover and meadow. Furthermore, the shady slope is covered by forest. Thus,  $L_t$  is given as (Lu et al.):

$$L_t = 0.5(1 - V_f) [F \sigma_{ss} \delta T_{ss}^4 + (1 - F) \sigma_g \delta T_g^4] + 0.5(1 - V_f) \sigma_c \delta T_c^4 \tag{11}$$

where  $T_c$  is the canopy temperature and is assumed to be equal to air temperature;  $\sigma_{ss}$  is the dimensionless effective emissivity for snow (0.98);  $\sigma_g$  is the dimensionless effective emissivity for the ground without snow cover (0.94);  $T_{ss}$  and  $T_g$  are

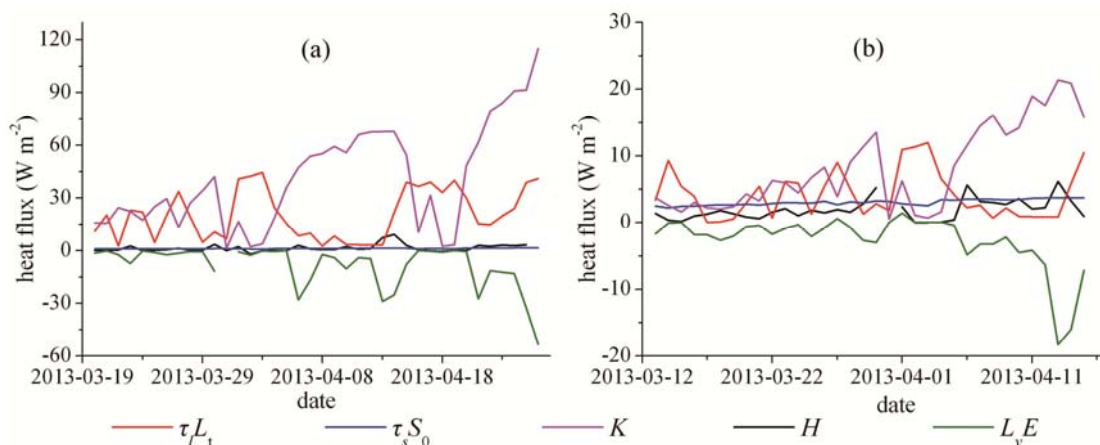


**Figure 9** The net radiation ( $K$ ), sensible heat flux( $H$ ), latent heat flux( $L_v E$ ), the longwave radiation due to the canopies heated above the air temperature because of the absorbed shortwave radiation( $\tau_s S_o$ ) and the longwave radiation enhanced by adjacent terrain( $\tau_l L_t$ ) beneath forest canopy on the shady slope, (a) beneath 80% forest canopy openness, (b) beneath 20% forest canopy openness.

the snow surface temperature and ground surface temperature of the area without snow cover.  $T_{ss}$  and  $T_g$  can be calculated with air temperature as (if  $T_{ss}$  calculated according to Eq.(12) exceeded  $0^{\circ}\text{C}$ , the  $T_{ss}$  was adjusted to  $0^{\circ}\text{C}$ ):

$$T_{ss}=0.9937T_a-2.8776 \quad (12)$$

$$T_g=1.6021T_a-2.2472 \quad (13)$$

Figure 10 shows the variation of  $L_t$  above forest canopy under different  $T_a$ ,  $V_f$ , and  $F$  conditions. The  $L_t$  increases with air temperature rise and the decrease of  $V_f$ . When the air temperature is relatively low, the influences of  $V_f$

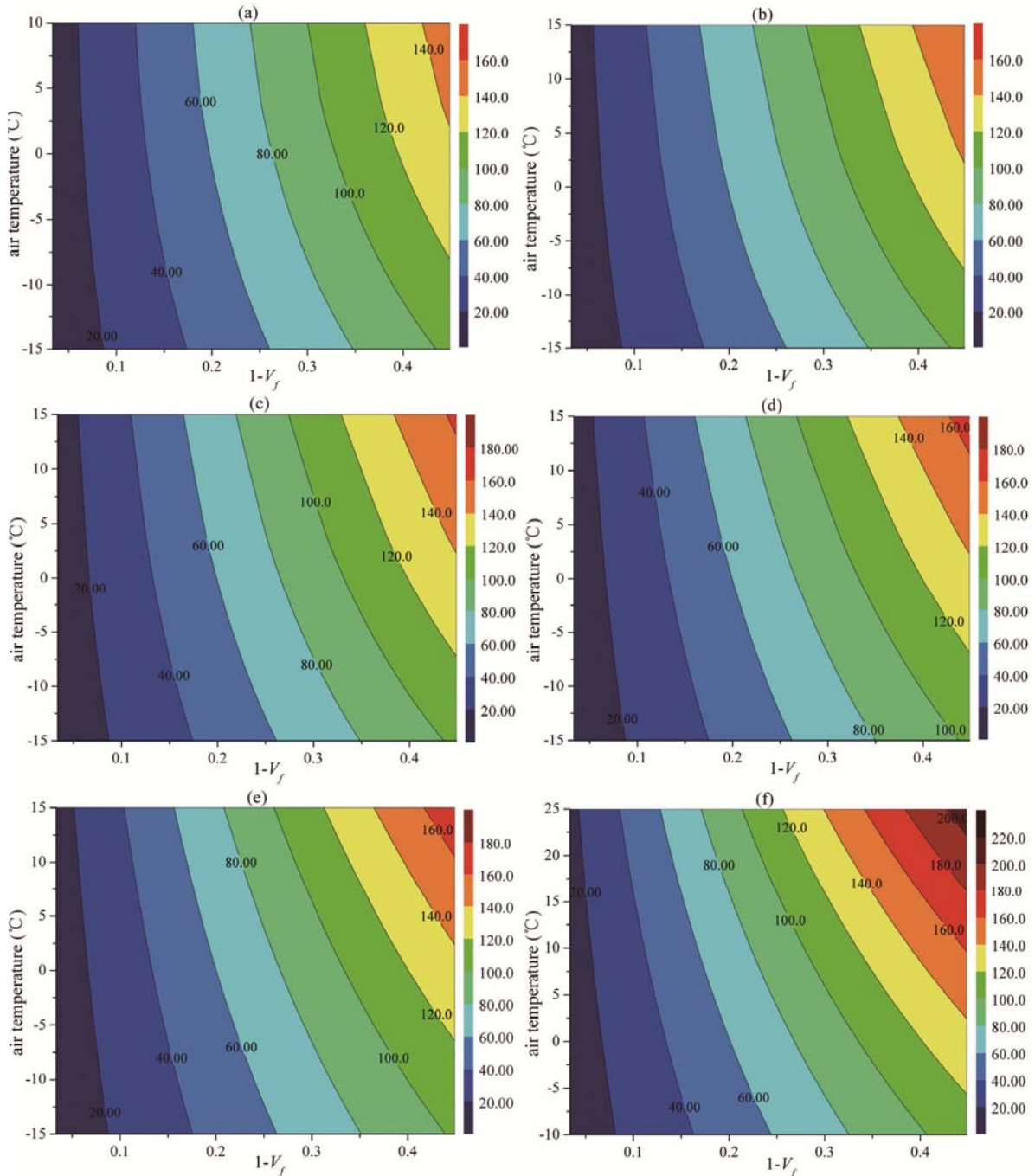


**Figure 10** The downward longwave radiation above forest canopy enhanced by adjacent terrain ( $L_t$ ) under different percentage of snow cover area ( $F$ ) conditions, (a) the sunny slope all covered by snow ( $F=100\%$ ), (b) 80% area of sunny slope covered by snow ( $F=80\%$ ), (c) 60% area of sunny slope covered by snow ( $F=60\%$ ), (d) 40% area of sunny slope covered by snow ( $F=40\%$ ), (e) 20% area of sunny slope covered by snow ( $F=20\%$ ), (f) the sunny slope did not have snow cover ( $F=0\%$ ).

and  $F$  on  $L_t$  are not significant, but the influences increase with air temperature rise. When the  $V_f$  is relatively high, the influence of air temperature and  $F$  on  $L_t$  is not significant, but the influences increase with the decrease of  $V_f$ . The influences of air temperature and  $V_f$  on  $L_t$  increase with the decrease of  $F$ . Especially, when the snow cover on the sunny slope melts completely ( $F=0$ ), air temperature rises rapidly and the  $L_t$  is very sensitive to the changes of the  $T_g$  and air temperature (Figure 10e).

For the wind speed beneath forest canopy on the shady slope was small, the variations of air temperature and humidity were less than those at open site on the sunny slope. Therefore, the influences of the changes of air temperature and humidity on the energy budget over snow surface beneath forest canopy were relatively small. For the end time of snowmelt period at the open site on the sunny slope was about 20~30 days earlier than that beneath forest canopy (Table. 1, Figure 6), the  $F=0$  when the snow melt beneath forest canopy on the shady slope. In the study area, the adjacent terrain is rugged; the slopes of sunny and shady slopes are general about 30°; the  $V_f$  is general about 0.8. Although  $\tau_l$  beneath 20% forest canopy openness was only 0.130, the increase of  $T_g$  on the sunny slope was larger than the increase of air temperature at the open site on the sunny slope. The increase of air temperature beneath forest canopy on the shady slope was the least. Moreover, the  $\sigma_g$  and  $\sigma_e$  were significantly larger than  $\sigma_a$ . Therefore the influence of ground surface temperature of adjacent terrain on the energy budget over snow surface beneath forest canopy was more significant than the influence of air temperature. The larger forest canopy openness and the steeper adjacent terrain indicate the more notably influence of ground surface temperature of adjacent terrains on energy budget over the snow surface beneath forest canopy.

#### 4 Conclusions

In different years, during the snowmelt period,  $K$  and  $H$  were energy source and  $L$  and  $L_vE$  were energy sinks at OPS. The  $K$  at BFC was significantly

lower than that at OPS due to the influences of vegetation and terrain. The gain of  $H$ , losses of  $L$  and  $L_vE$  at BFC were also lower than that at OPS. The smaller the forest canopy openness was, the lower the  $K$  value was. The  $L$  was the maximum difference of energy budget between snow surface at BFC and snow surface at OPS. The  $L$  at 20% BFC was even positive. Although the radiation was the most important energy source over snow surface at all sites, the percentage of radiation *vis-à-vis* energy gain at BFC was clearly greater than that at OPS. The longwave radiation enhanced by adjacent terrain ( $\tau_l L_t$ ) over snow surface was higher than  $H$  and  $L_vE$ , and even higher than  $K$  over snow surface at BFC during the earlier snowmelt period or in precipitation days. The influence of ground surface temperature of adjacent terrain increased with the decrease in  $F$ , especially when the  $F=0$ .

Against the background of a warming and humid climate in the western Tianshan Mountains, the humidity increase is the most important factor for the variation of the energy budget over snow surface at OPS. The  $H$  increase with air temperature rise is the second important factor. Moreover, the change of  $H$  is influenced by the air temperature rise pattern in the daytime and nighttime. For the wind speed is relatively low at BFC and the effects of vegetation and terrain, the influences of ground surface temperature rise of adjacent terrain on energy budget is more significant than the influences of air temperature and humidity rise on energy budget over snow surface at BFC. The larger forest canopy openness and the steeper adjacent terrain indicate the more significant response of the energy budget over snow surface beneath forest canopy to ground surface temperature rise of adjacent terrain.

#### Acknowledgement

The research presented in this article was jointly funded by the National Natural Science Foundation of China (41271098, 41171066), and the National Key Technology Research and Development Program of the Ministry of Science and Technology of China (2012BAC23B01).

## References

- Aizen V, Aizen E, Melack J (1997) Snow distribution and melt in central Tien Shan, Susamir Valley. *Arctic and Alpine Research* 29(4): 403-413.
- Anderson E (1976) A point energy and mass balance model of a snow cover. Office of Hydrology, National Weather Service, Silver Spring, Maryland, NOAA Technical Report NWS 19.
- Barnett TP, Adam JC, Lettenmaier DP (2005) Potential impacts of a warming climate on water availability in snow-dominated regions. *Nature* 438: 303-309. DOI: 10.1038/nature04141
- Bao AM, Chen XN, LI L (2010) Theories and methods of snowmelt runoff and its application in arid regions. *Arid Land Geography* 33(5): 684-691. (In Chinese)
- Boon S (2009) Snow ablation energy balance in a dead forest stand. *Hydrological processes* 23: 2600-2610. DOI: 10.1002/hyp.7246
- Burles K, Boon S (2011) Snowmelt energy balance in a burned forest plot, Crowsnest Pass, Alberta, Canada. *Hydrological processes* 25(19): 3012-3029. DOI: 10.1002/hyp.8067
- Calanca P, Heuberger R (1990) Energy balance. In: *Glacial Climate Research in the Tianshan, research report on project Glacier No.1*. Ohmura A et al. (eds.), Zurcher Geographische Schriften, No. 38. Geographisches Institut, ETH, pp 60-70.
- Che T, Li X (2005) Spatial distribution and temporal variation of snow China During 1993- 2002. *Journal of Glaciology and Geocryology* 27(1): 64-67. (In Chinese)
- Cline DW (1997) Effect of seasonality of snow accumulation and melt on snow surface energy exchange at a continental alpine site. *Journal of Applied Meteorology* 36: 32-51. DOI: 10.1175/1520-0450(1997)036<0032:EOSOSA>2.0.CO;2
- de la Casiniere AC (1974) Heat exchange over a melting snow surface. *Journal of Glaciology* 13: 55-72.
- Essery R, Pomeroy J, Ellis C, et al. (2008) Modelling longwave radiation to snow beneath forest canopies using hemispherical photography or linear regression. *Hydrological processes* 22(15): 2788-2800. DOI: 10.1002/hyp.6930.
- Harding R, Pomeroy J (1996) The energy balance of the winter boreal landscape. *Journal of Climate* 9: 2778-2787. DOI: 10.1175/1520-0442(1996)009<2778:TEBOTW>2.0.CO;2
- Hay J, Fitzharris B (1988) A comparison of energy balance and bulk aerodynamic approaches for estimating glacier melt. *Journal of Glaciology* 34(117): 145-153.
- Hock R, Holmgren B (2005) A distributed surface energy-balance model for complex topography and its application to Storglaciaren, Sweden. *Journal of Glaciology* 51(172): 25-36. DOI: 10.3189/172756505781829566
- Hu RJ, Ma H, Jiang FQ (1997) Geographical environment in the area of Tianshan Station for Snow & Avalanche Research, Yili, Xinjiang, China. *Arid Land Geography* 20(2): 25-33. (In Chinese)
- Grainger M, Lister H (1966) Windspeed, stability and eddy viscosity over melting ice surface. *Journal of Glaciology* 6(43): 101-127.
- Iziomon M, Mayer H, Matzarakis A (2003) Downward atmospheric longwave irradiance under clear and cloudy skies: Measurement and parameterization. *Journal of Atmospheric and Solar-Terrestrial Physics* 65(10): 1107-1116. DOI: 10.1016/j.jastp.2003.07.007.
- Jin J, Gao XG, Sorooshian S, et al. (1999) One-dimensional snow water and energy balance model for vegetated surfaces. *Hydrological Processes* 13: 2467-2482. DOI: 10.1002/(SICI)1099-1085(199910)13:14/15<2467::AID-HYP861>3.0.CO;2-J
- Liu ZC, Sun L, Cai GT (1989) Research results of snowcover radiation equilibrium in the western hill area of Tianshan, China. *Arid Land Geography* 12(4): 37-42. (In Chinese)
- Liu MZ, Wei WS, Jiang FQ (1997) On the characteristics of energy exchange of winter snow cover in western Tianshan mountains. *Arid Land Geography* 20(4): 68-73. (In Chinese)
- Lu H, Wei WS, Liu MZ, et al. (2014) Observations and modeling of incoming longwave radiation to snow beneath forest canopies in the west Tianshan Mountains, China. *Journal of Mountain Science* 11(5): 1138-1153. DOI: 10.1007/s11629-013-2868-1
- Ma H, Liu ZC, Liu Y (1992) Energy balance of a snow cover and simulation of snowmelt in the western Tien Shan Mountains, China. *Annual of Glaciology* 16: 73-78.
- Ma H, Liu YF, Hu RJ (1993) Energy balance and snowmelt simulation of seasonal snow in the Western Tianshan Mountains, China. *Geographical Research* 12(1): 87-93. (In Chinese)
- Male D, Gray D (1981) *Handbook of Snow, Principles, Processes, Management and Use*. Pergamon Press, Toronto, Canada. pp 360-436.
- Marks D, Dozier J (1992) Climate and energy exchange at the snow surface in the alpine regions of the Sierra Nevada. Part III. Snow cover energy balance. *Water Resource Research* 28(11): 3043-3053. DOI: 10.1029/92WR01483
- McGregor GR, Gellatly AF (1996) The energy balance of a melting snowpack in the French Pyrenees during warm anticyclonic conditions. *International Journal of Climatology* 16(4): 479-486. DOI: 10.1002/(SICI)1097-0088(199604)16:4<479::AID-JOC17>3.0.CO;2-W
- McKay DC, Thurtell GW (1978) Measurements of the energy fluxes involved in the energy budget of a snow cover. *Journal of Applied Meteorology* 17(3): 339-349.
- Moore RD, Owens IF (1984) Controls on advective snowmelt in a maritime alpine basin. *Journal of Applied Meteorology* 23: 135-142. DOI: 10.1175/1520-0450(1978)017<0339:MOTEFI>2.0.CO;2
- Munro DS (1989) Surface roughness and bulk heat transfer on a glacier: comparison with eddy correlation. *Journal of Glaciology* 35(121): 343-348.
- Neale S, Fitzharris B (1997) Energy balance and synoptic climatology of a melting snowpack in the Southern Alps, New Zealand. *International Journal of Climatology* 17(14): 1595-1609. DOI: 10.1002/(SICI)1097-0088(19971130)17:14<1595::AID-JOC213>3.0.CO;2
- Price A, Dunne T (1976) Energy balance computations of snowmelt in a subarctic area. *Water Resources Research* 12(4):686-694. DOI: 10.1029/WR012i004p00686
- Qin D, Liu S, Li P (2006) Snow cover distribution, variability, and response to climate change in Western China. *Journal of Climate* 19: 1820-1833. DOI: 10.1175/JCLI3694.1
- Rowlands A, Pomeroy J, Hardy J, et al. (2002) Small-scale spatial variability of radiant energy for snowmelt in a mid-latitude sub-alpine forest. 2002. Proceedings from the 59<sup>th</sup> Eastern Snow Conference. pp 109-117.
- Sensoy A, Sorman AA, Tekeli AE, et al. (2006) Point-scale energy and mass balance snowpack simulations in the upper Karasu basin, Turkey. *Hydrological Processes* 20: 899-922. DOI: 10.1002/hyp.6120
- Shi YF, Shen YP, Hu RJ (2002) Preliminary study on signal, impact and foreground of climatic shift from warm-dry to warm-humid in Northwest China. *Journal of Glaciology and Geocryology* 24(3): 219-226. (In Chinese)
- Shi YF, Shen YP, Li DL, et al. (2003) Discussion on the present climate change from warm-dry to warm-wet in Northwest China. *Quaternary Sciences* 23(2): 152-164. (In Chinese)
- Sicart JE, Essery RL, Pomeroy JW, et al. (2004) A sensitivity study of daytime net radiation during snowmelt to forest canopy and atmospheric conditions. *Journal of Hydrometeorology* 5(5): 774-784. DOI: 10.1175/1525-7541(2004)005<0774:ASSODN>2.0.CO;2
- Sicart J, Pomeroy J, Essery R, et al. (2006) Incoming longwave radiation to melting snow: observations, sensitivity and estimation in northern environments. *Hydrological processes* 20(17): 3697-3708. DOI: 10.1002/hyp.6383.

- Sverdrup HU (1936) The eddy conductivity of the air over a smooth snow field. *Geofysiske Publikasjoner* 11(7): 1-69.
- Suzuki K, Ohta T (2003) Effect of larch forest density on snow surface energy balance. *Journal of Hydrometeorology*, 4(6): 1181-1193. DOI: 10.1175/1525-7541(2003)004<1181:EOLFD0>2.0.CO;2
- Tarboton DG, Chowdhury TG, Jackson TH (1995) A spatially distributed energy balance snowmelt model. *IAHS Publ No.* 228. pp 141-155.
- Viviroli D, Durr H, Messerli B, et al. (2007) Mountains of the world, water towers for humanity: Typology, mapping, and global significance. *Water Resource Research* 43(1): 1-13. DOI: 10.1029/2006WR005653
- Wei WS, Wang CN, Jiang FQ, et al. (1996) Studies on the processes of thermal exchange, evaporation and sublimation of the snow cover in the Tianshan Mountains, China. *Journal of Glaciology and Geocryology* 18(S1): 129-138. (In Chinese)
- Wei WS, Yuan YJ, YU SL, et al. (2008) Climate change in recent 235 years and trend prediction in Tianshan Mountains areas. *Journal of Desert Research* 28(5): 803-808. (In Chinese)
- Xu JR, Chou JQ (1996) A study on snowfall variation in the Tianshan Mountains during the recent 30 winters. *Journal of Glaciology and Geocryology* 18: 123-138. (In Chinese)
- Yang Q, Cui CX, Sun CR (2007) Snow cover variation in the past 45 years (1959-2003) in the Tianshan Mountains, China. *Advances in Climate Change Research* 3(2): 80-84. (In Chinese)
- Yao JQ, Yang Q, Zhao L (2012) Research on change of surface water vapor in the Tianshan Mountains under global warming. *Arid Zone Research*, 29(2): 320-327. (In Chinese)
- Yuan YG, He Q, Wei WS, et al. (2003) Comparison of features of annual temperature change in Tianshan Mountains area, Southern and Northern Xinjiang for recent 40 years. *Journal of Desert Research* 23(5): 521-526. (In Chinese)
- Zhang Z, Liu P, Ding Y, et al. (2010) Species compositions and spatial distribution pattern of tree individuals in the schrenk spruce forest, northwest China. *Journal of Nanjing Forestry University (Natural Science Edition)* 34: 157-160. (In Chinese)